mathematics

Article

Numerical Investigation of Wind Flow and Speedup Effect at a Towering Peak Extending out of a Steep Mountainside: Implications for Landscape Platforms

Mohammed Nabil , Fengqi Guo *, Lizhong Jiang, Zhiwu Yu and Qiuliang Long

School of Civil Engineering, Central South University, Changsha 410075, China; monabil@csu.edu.cn (M.N.)
* Correspondence: fengqiguo@csu.edu.cn

Abstract: Wind flow over complex terrain is strongly influenced by the topographical features of the region, resulting in unpredictable local wind characteristics. This paper employs numerical simulation to study the wind flow at a towering peak extending out of a steep mountainside and the wind-induced effect on onsite landscape platforms. First, the wind flow from seven different directions is explored via 3D numerical simulations, and the wind load distribution on the platforms is highlighted. Second, a 2D numerical simulation is conducted to evaluate the wind speedup effect at the side peak, examining the influence of the side peak height and the mountainside steepness on the wind speedup factor. The numerical simulations presented in this research were validated by replicating a published numerical and experimental study. The results illustrate the amplifying and blocking effects of the surrounding topography, yielding unpredictable and nonuniform wind pressure distribution on the platforms. The presence of the side peak leads to a significant increase in the speedup factor, and the side peak height and the mountainside steepness have a moderate influence on the value of the speedup factor. Additionally, the speedup factor obtained from this study varies significantly, especially near the surface, from the recommendations of several wind load standards. Consequently, the impact of the local terrain and the wind speedup effect must be thoroughly assessed to ensure the structural integrity of structures installed at a similar topography.

Keywords: numerical simulation; speedup factor; computational fluid dynamic; complex structure; simulation accuracy

MSC: 74F10; 76F40

check for updates

Citation: Nabil, M.; Guo, F.; Jiang, L.; Yu, Z.; Long, Q. Numerical Investigation of Wind Flow and Speedup Effect at a Towering Peak Extending out of a Steep Mountainside: Implications for Landscape Platforms. *Mathematics* **2024**, *12*, 467. https://doi.org/10.3390/math12030467

Academic Editor: Sergey Ershkov

Received: 8 January 2024
Revised: 26 January 2024
Accepted: 29 January 2024
Published: 1 February 2024

1. Introduction

The atmospheric boundary layer (ABL) over mountainous regions is significantly affected by the local topography, resulting in its complex behavior. This complexity poses challenges for scientists and engineers who require comprehensive evaluations of the wind field within the relevant terrains. Moreover, this need becomes even more pronounced with the escalating expansion of human projects—such as transportation infrastructures and wind farms—into intricate regions. Over the past few decades, scholars have relied on field measurements to extract local wind data. However, this approach poses certain economic and technical challenges, especially when studying the wind field at a larger scale. Researchers have employed alternative methods, primarily wind tunnel tests and numerical simulations, to overcome these limitations.

Recent significant technological advancements, combined with the constant improvement in computational fluid dynamics (CFD) software, have promoted the utilization of numerical simulations to investigate wind field characteristics over mountainous valleys. Hu et al. [1] numerically studied the wind flow over hilly terrain and proposed a novel turbulence generating method. The numerical simulation successfully predicted the wind field characteristics over realistic hilly terrain and three-dimensional hills with different slopes. Song et al. [2] conducted numerical simulation for the wind field in complex terrain. The results were validated by the wind tunnel test, and it was established that the k-models produced superior predictions to those of other RANS models. Blocken et al. [3] utilized CFD simulation and field measurements to evaluate the wind characteristics in intricate terrains. The results obtained by applying the steady realizable k-ε model show great consistency with the experimental data. Moreira et al. [4] assessed the ability of various RANS turbulence models to simulate airflow over the complex terrain of Askervein Hill accurately. Han et al. [5] proposed a multiscale coupling approach suitable for determining the inlet mean wind speed for numerical simulations of the wind field in mountain gorges. In addition to conducting CFD simulations of wind fields in natural topography, researchers have extensively studied wind flow over typical circular hills [6–9].

The intricate nature of real terrains often subjects the wind flow to a speeding-up effect, a phenomenon that has been extensively discussed by many scholars [10–13]. Flay et al. [14] conducted a comprehensive investigation of the speedup effect in the Belmont Hill region to enhance wind speed predictions. This study involved a comparison of various national wind standards with speedup predictions based on field observations. Chen et al. [15] utilized wind tunnel tests and numerical simulations to assess the speedup effect at the peaks of coastal island mountains, and the influence of the large-scale topography on the speedup effect was highlighted. Pirooz et al. [16] performed numerical simulations for 2D and 3D bell-shaped hills to evaluate the accuracy of speedup multipliers suggested by various wind load standards. The results, validated by a wind tunnel test, revealed certain variations from the recommended values.

Despite abundant research focusing on the wind flow around and through structures on flat surfaces [17–19], understanding the wind-induced effects on structures in complex terrains remains inadequate. Meng et al. [20] conducted a CFD simulation for a tall building with a rectangular section in relatively complex topography. The study revealed significant negative pressure on the building's side surfaces caused by flow separation induced by the front terrain. Han et al. [21] employed numerical simulation to evaluate the impact of surrounding hilly terrain on the wind-induced pressure of a traditional temple within a complex terrain. Lee-Sak et al. [22] conducted wind tunnel tests to assess the influence of terrain complexity on the wind load of low-rise buildings. The experiment also highlighted the effect of terrain roughness on wind flow characteristics such as turbulence intensity.

In the last few decades, the Chinese economy and local individuals' incomes have grown exponentially. This growth led to a significant expansion in the local tourism industry. Many local governments and businesses have capitalized on the local natural features, including hills, waterfalls, and forests, to leverage this growth and attract the largest possible number of visitors. This study presents a comprehensive 3D and 2D simulation investigation of the wind field at a towering peak protruding from a steep mountainside, as depicted in Figure 1. This peak serves as the site for a front butterfly-lookalike landscape platform, which will be connected—via a glass bridge over a narrow col—to a second platform on the mountainside. This platform will hover over the astonishing landscapes of Dajue Mountain, becoming a new tourist attraction and contributing to the region's economic growth.

As ecotourism gains popularity, the emergence of structures in similar locations is expected to increase. Given the limited existing research on the wind loads experienced by complex structures at unique sites, such as towering peaks, a thorough investigation of the local wind field and its impact on structures is highly needed. This research aims to enhance the understanding of the wind flow around architecturally sophisticated structure and analyze the influence of surrounding topography on its behavior. The study provides essential information for designing engineers to ensure the stability of the structure under various wind speeds and directions. Additionally, the research evaluates the speedup effect at the side peak, emphasizing the impact of the side peak height and the mountainside steepness on the speedup factor. The CFD simulation results are compared to the recommendations of several national wind load standards. This investigation holds practical merit and offers valuable guidance for relevant future research. The remainder of this paper is as follows: Section 2 presents numerical simulations of the wind flow over complex terrain, focusing on the impact of the surrounding topography on the platforms wind-induced pressure. Section 3 examines the speedup effect at the side peak and the influence of different side peak heights and mountainside slopes. Section 2 lists the findings of this research.

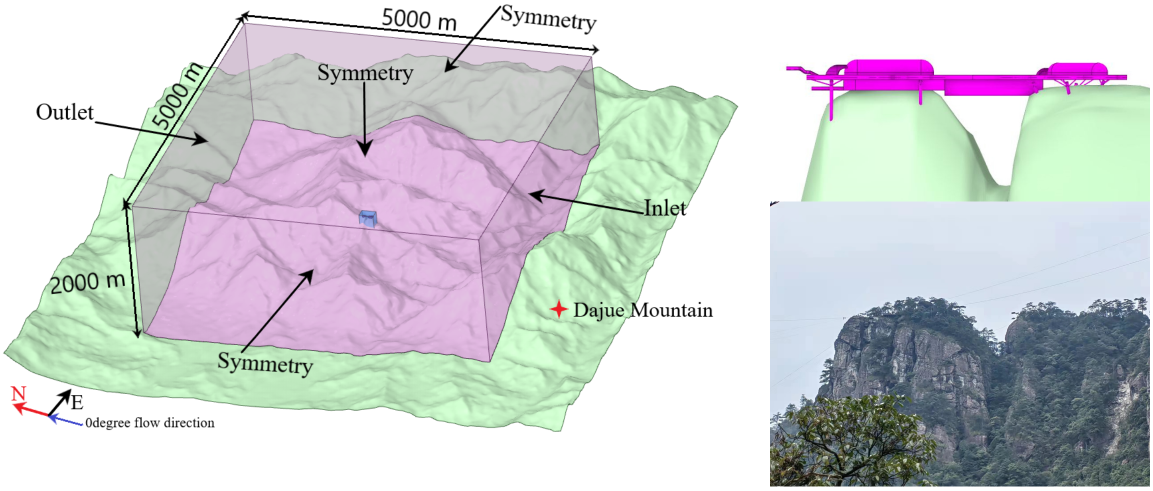

Figure 1. The local topography and 3D model of the computational domain and platforms.

2. 3D Numerical Simulation

2.1. Computational Domain and Flow Directions

The targeted simulation domain is within Dajue Mountain Jiangxi Province, China. The side peak stands at approximately 90 m on the steep mountainside. This towering peak is isolated from the main body of the mountain by a narrow col with a width of 10 m. The steel butterfly-lookalike landscape platforms have maximum dimensions of 60 m in length and 75 m in width. The overall height of the platform is 29 m, and the glass bridge spans a length of 40.5 m, as illustrated in Figure 1.

The model of the local topography of Dajue Mountain was generated using digital elevation model (DEM) data provided by NASA, with a resolution of 12.5 m per pixel. The contour lines of the region were extracted by Global Mapper, and the terrain surface was modeled using Rhinoceros. The platform models were created in Ansys SpaceClaim (2021 R1) based on the provided architectural drawings.

According to available wind field observations, the wind flow mainly blows at high speeds from the south and the west. Furthermore, the mountain body blocks the wind flow from the north, leading to a significant decrease in the wind speed to less than 2 m/s at the platforms site, as shown in Figure 2. Consequently, this study did not investigate the wind flow from the direct north. The other seven wind directions, every 45 degrees, are studied with the initial case (0 degrees) signifying the flow from the south. Additionally, the numerical simulations are conducted on scaled models at a ratio of 1/100.

2.2. Mesh Arrangement

Mesh settings highly influence the wind field numerical simulation results, and poor mesh quality could prevent the convergence of the solution. To address this, scholars have introduced various meshing guidelines, including the aerodynamic roughness suggested by Blocken et al. [23]. In this context, the aerodynamic roughness of the terrain surface is represented by an equivalent sand grain size k_S, and the height of the first mesh layer cannot be less than 6 m, according to Equation (1).

$$k_s = \frac{9.793 z_0}{C_s} \tag{1}$$

$$k_s = 29.6z_0 \quad (2)$$

where $z_0 = 0.05$ is the roughness height, and $C_s = 0.16$ is the roughness constant according to the Chinese wind resistance code [24].

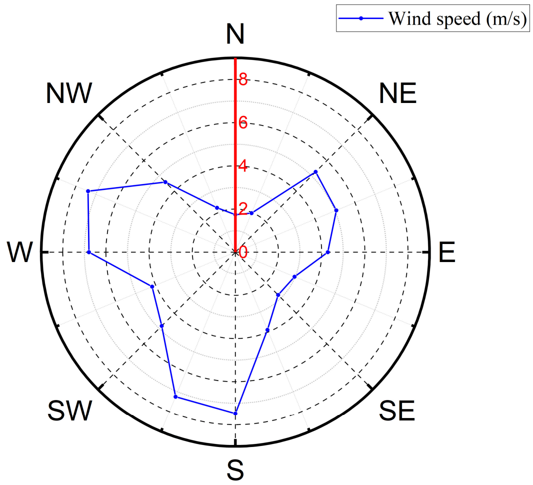

Figure 2. Mean wind speed and direction.

Currently, researchers are utilizing several software and tools, such as Gambit and Ansys ICEM tool, to generate mesh for wind field numerical simulation. However, due to the geometric complexity of the landscape platforms and the natural terrain, Ansys (Fluent meshing) (2021 R1) was used to generate the mesh, and the poly-hexacore mesh type was chosen, as shown in Figure 3. Selecting an appropriate mesh arrangement is a repetitive process that takes into account the simulation equality and calculation time requirements. In this study, a grid independence test was conducted to select the ideal mesh scheme, and three approaches with total mesh cell numbers of 11.0, 16.7, and 23.2 million were examined. The test showed that the maximum wind speed difference of the three schemes at the front platform was only 2.64%, as illustrated in Figure 4. Consequently, the second scheme with 16.7 million mesh cells was applied for the subsequent simulations. In this grid arrangement, the inner domain surrounding the platforms has a maximum cell length of 1 m, and the entire simulation domain has mesh cells with minimum and maximum lengths of 0.1 m and 50 m, respectively. This wide mesh size range ensures that the minor details of complex geometry are captured while keeping the calculation time manageable.

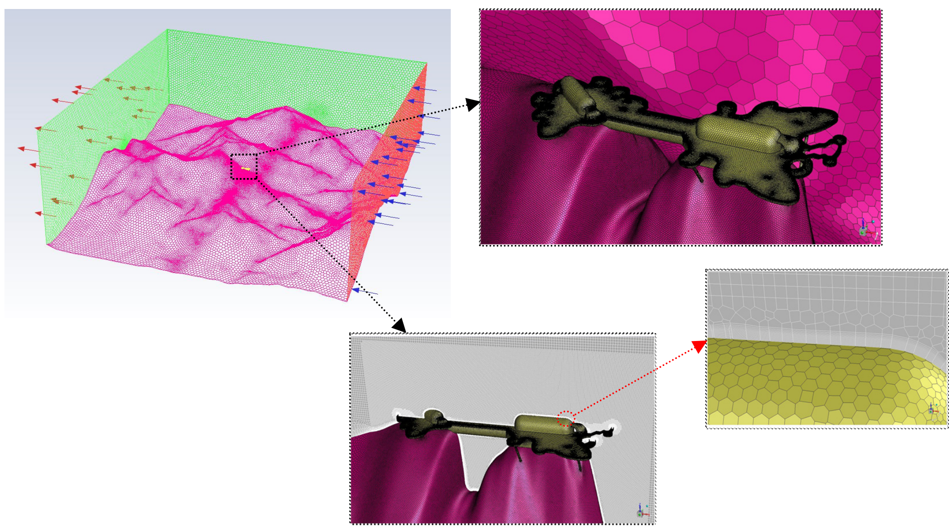

Figure 3. Computational grid.

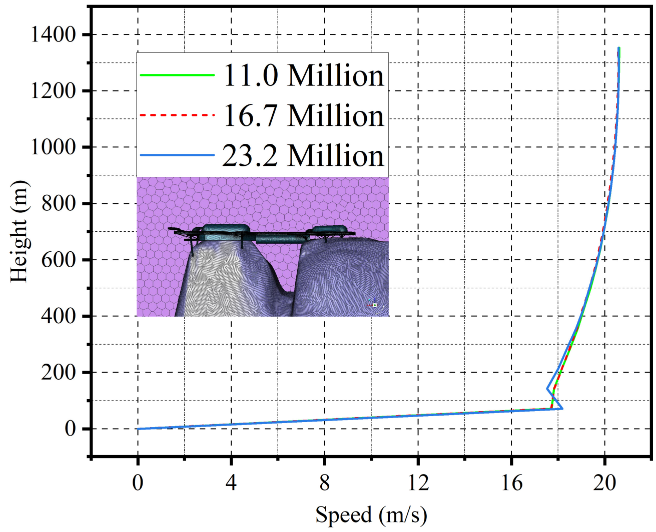

Figure 4. Mesh independency test.

2.3. Atmosphere Boundary Layer and Boundary Conditions

The atmospheric boundary layer (ABL) numerical simulation has been of great interest to researchers, and the currently common approaches involve wall-shear-driven and pressure-driven models. However, since the wind flow within the ABL is generated primarily through differences in regional atmospheric pressure, many scholars have utilized pressure-driven models to simulate the airflow over natural topographies. Additionally, the accuracy of this approach in predicting wind field characteristics in complex terrains has been validated via comparisons with wind tunnel tests and field measurements [16]. This study utilized the pressure-driven mathematical model developed by Deaves and Harris [25] as follows:

$$U(z) = \frac{u^*}{\kappa}\left(\ln\left(\frac{z}{z_0}\right) + 5.75\left(\frac{z}{h}\right) - 1.875\left(\frac{z}{h}\right)^2 - 1.333\left(\frac{z}{h}\right)^3 + 0.25\left(\frac{z}{h}\right)^4\right) \tag{3}$$

where u^* is the fraction velocity, $\kappa = 0.4$ is the Von Karman constant, h is the gradient height, and f is the Coriolis parameter.

$$h = \frac{u^*}{6f} \tag{4}$$

The turbulence model applied in this research is the (k-ε; Realizable) model, and the inlet profile is defined according to Richards and Norris [26] as follows:

$$U(z) = \frac{u^*}{\kappa}\left(\ln\left(\frac{z}{z_0}\right) + C_{U1}\left(\frac{z}{H}\right) + C_{U2}\left(\frac{z}{H}\right)^2 + C_{U3}\left(\frac{z}{H}\right)^3 + C_{U4}\left(\frac{z}{H}\right)^4\right) \tag{5}$$

$$k(z) = u^{*2}\left(C_{k1} + C_{k2}\left(1 - \frac{z}{H}\right)^2 + C_{k3}\left(1 - \frac{z}{H}\right)^4 + C_{k4}\left(1 - \frac{z}{H}\right)^6\right) \tag{6}$$

$$\varepsilon(z) = \frac{C_\mu k(z)^2}{\kappa u^* z}\left(1 + (1 + C_{U1})\left(\frac{z}{H}\right) + (1 + C_{U1} + 2C_{U2})\left(\frac{z}{H}\right)^2 + (1 + C_{U1} + 2C_{U2} + 3C_{U3})\left(\frac{z}{H}\right)^3\right) \tag{7}$$

$$\tau = \rho u^{*2} \tag{8}$$

where $U(z)$ is the wind speed, $k(z)$ is the turbulence kinetic energy, $\varepsilon(z)$ is the turbulence dissipation rate, τ is the wall shear stress, and $\rho = 1.225$ kg m^{-3} is the air density. The values of the constants mentioned in Equations (5)–(7) were previously calculated by Richards and Norris [26].

The symmetry boundary condition is assigned to the top and side surfaces, and the pressure outlet boundary condition with zero-gauge pressure is applied at the outlet of the domain. The terrain's surface and platforms are selected as no-slip walls, and the surface roughness of the terrain due to the vegetation cover is represented by the corresponding wall function parameters k_S and C_S, as in Equation (1). This method simulates the impact of the forest on the airflow development throughout the domain by altering the surface initial roughness length z_0 with the equivalent sand grain size roughness height k_S. Additionally, this approach is widely applied by researchers, and has produced high-quality wind numerical simulations [3]. Furthermore, the scalable wall function is applied to the terrain surface to ensure the accuracy of the near-ground wind simulation. The airflow simulated in this study maintains the initial settings of Ansys Fluent, with a density of 1.225 kg m^{-3}. The simulation convergence criteria were set to 1×10^{-6}, and the solution reached stability within 5000 steps.

2.4. Results

The results obtained from the 3D numerical simulation conducted using Ansys Fluent (2021 R1) are presented in this section, and the impact of the local terrain on the wind-induced effects on the platforms is highlighted.

2.4.1. Platforms Wind-Induced Effects

The platforms' wind-induced pressure resulting from the wind flow from seven different directions is depicted in Figure 5 and Figure 7. The figures show that the sides of the platform facing the wind flow direction experience significant pressure and lifting forces. This effect is particularly evident in Cases 5 and 6, where the wind-induced positive pressure reaches a maximum value of approximately 750 Pa. This is attributed to the relatively open topography of the western and northwestern regions of the terrain. As in Case 6, the wind flow experienced a speeding-up effect by the relatively shorter mountain in the west. In Case 7, the northwestern mountains redirected the wind flow toward the side peak, resulting in higher wind pressure. However, due to the shading effect of the mountains in the northeast direction (Case 4), the platforms, especially the one on the mountainside, were subjected to a significant negative wind pressure. This pressure results from the large vortex formed behind the mountains, attempting to lift the platforms off their bases.

Due to the complex shape of the landscape platforms and the unique installation location, a towering peak, the wind flow undergoes critical separation, resulting in local vortices, as depicted in Figure 6. The figure illustrates the wind flow streamlines from the west (Case 6) and northwest directions (Case 6). As can be seen, the wind flow from the west separates around the edges and domes of the platforms, creating small vortices. These vortices led to the nonuniform distribution of wind pressure on the platforms and the appearance of negative pressure. Furthermore, as the wind flow reattached, a positive wind pressure occurred on the other side of the platforms. This force distribution, coupled with the lifting forces resulting from the upwards redirected wind flow, imposes a significant torsional wind load on the platforms. This torsional effect threatens the structural stability of such lightweight metal structures, and under extreme weather conditions, this may cause uplift or detachment of the platforms' wings. Additionally, the glass bridge connecting the two platforms appears to be more susceptible to damage, and wind-induced vibrations may occur.

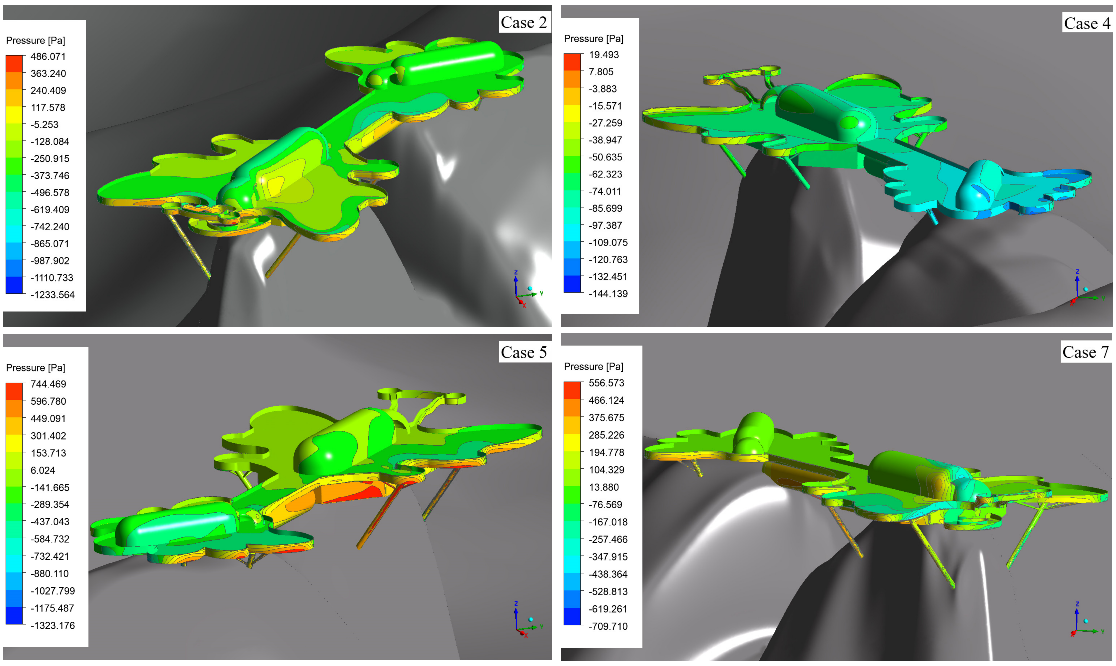

Figure 5. Platforms' mean surface pressure for Cases 2, 4, 5, and 7.

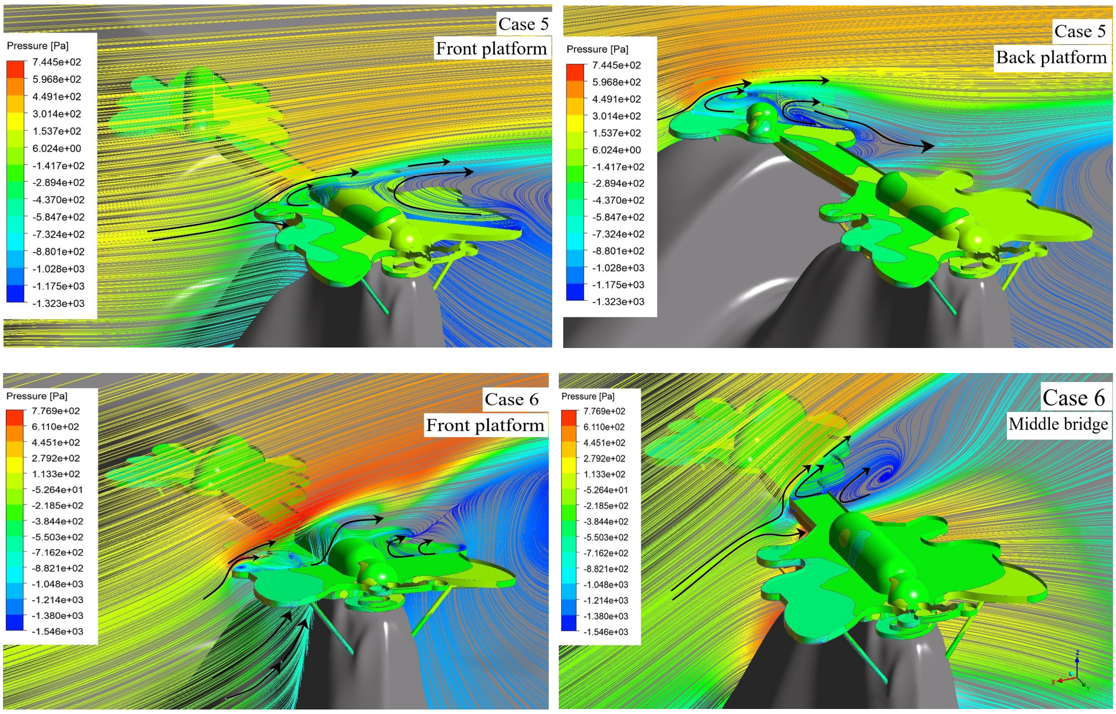

Figure 6. Streamlines of mean velocity for Cases 5 and 6.

2.4.2. Effect of Local Topography

The complex terrain surrounding the landscape platforms significantly influences the approaching airflow and plays a crucial role in determining the wind-induced effects on the structure. To closely examine the local topography effect, additional numerical simulations of the wind flow from the front and two sides of platforms on a plain surface were conducted. Furthermore, the same domain boundary conditions and mesh settings used for the real terrain are applied in these CFD simulations. The numerical simulation results of the wind flow over the real terrain and the plain surface are shown in Figure 7.

The figure demonstrates the substantial amplifying effect imposed by the local topography on the platforms' wind-induced pressure. The wind pressure shows a significant increase, reaching over five times that of the plain surface, particularly in Case 1 and Case 6, where the relatively open area of the terrain provides an unobstructed path for the speedup effect to occur. The following section extensively investigates the speedup effect at the site of the front platform under Case 1, and the findings predicted a speedup factor near the surface of around three. This threefold increase in the wind speed at the side peak is close to the observed pressure increase of around 3.5 times on the front face of the platform. This conclusion highlights the accuracy of the wind speedup effect predictions provided by the second half of this study.

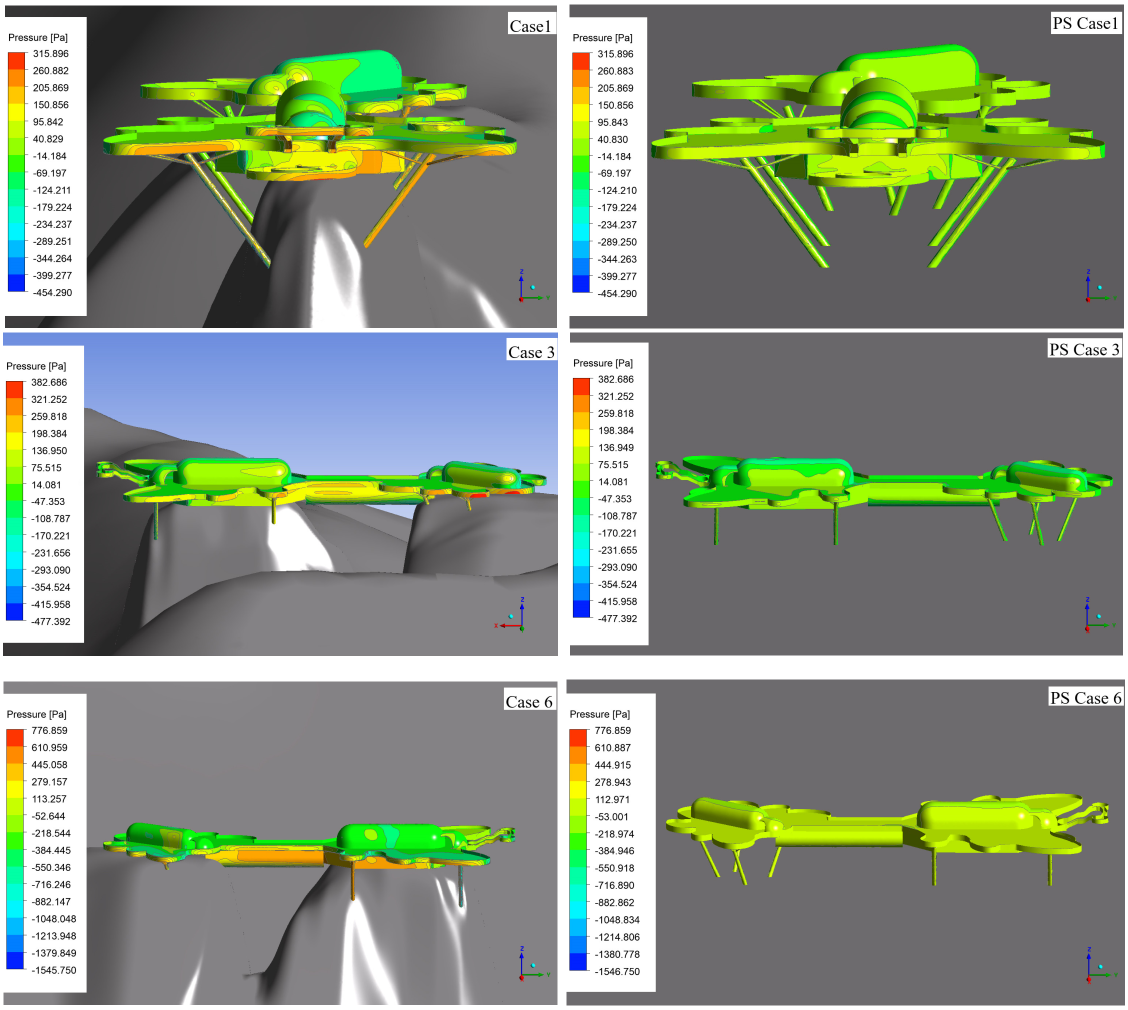

Figure 7. Platforms' mean surface pressure for Cases 1, 3, and 6.

Furthermore, the comparison reveals significant variations in the distribution of negative wind pressure, resulting in lifting and torsional forces. Therefore, a thorough evaluation of the wind behavior and the effect of the surrounding topography is highly recommended when undertaking construction projects or installing wind turbines at similar sites. Failing to do so may result in structural failure, especially under intense weather conditions and powerful storms.

3. Wind Speedup Effect

3.1. Wind Load Standards and Speedup Effect

The wind speedup factor refers to the ratio of the wind speed at a certain height above the hill or escarpment to the wind speed at the same height on flat ground. The wind speedup factor has proven essential in determining the wind load on structures in complex terrains. According to the previous investigation, the speedup phenomenon resulting from the local topography could significantly amplify the wind load on local structures, potentially causing unpredictable structural damage.

Many national wind load standards have addressed the wind speedup effect by introducing a topographic multiplier and developing straightforward mathematical approaches to calculating this multiplier. These calculations consider various factors, such as the height of the hill/escarpment and the horizontal distance from the hill's peak to the targeted hillside location. More explicit details regarding the calculation process can be found in the listed references. This study compares the speedup factor at the side peak obtained from 2D numerical simulations under different side peak heights (90 and 135 m) and mountainside slopes (0.2, 0.31, and 0.5), with the topography multipliers suggested by four wind load standards, namely AS/NZS 1170.2 (2021) [27], NBC-2020 [28], BS-EN (2005–2010) [29,30], and ASCE-7 (2022) [31].

3.2. Computational Domain and Grid

The mountain profile used for this simulation represents a vertical section at the side peak of the 3D model of the actual topography of Dajue Mountain, as shown in Figure 6. Furthermore, the mountain extends upwind to the valley's lowest point at 2185 m from the mountain peak. The overall height of the mountain is 685 m, and the side peak extends 90 m from the mountainside. Additionally, the front mountain, located over 2800 m from the side peak, was omitted and treated as a flat surface. This prevents the possible blocking effect of the distant mountain, which could disturb the wind flow and divert the results. As the backside of the mountain is not considered in this simulation, nor does it affect the speedup factor at the side peak, it was replaced by the Witozinsky transition curve [32] and positioned 720 m from the mountain peak. The dimensions of the computational domain are shown in Figure 8, and the scale ratio of the simulation model is 25:100.

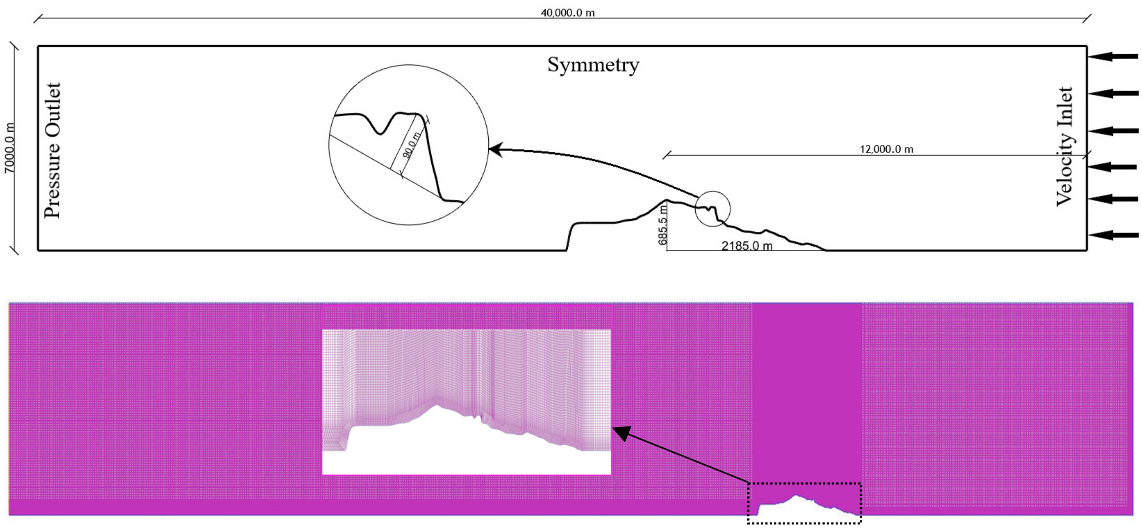

Figure 8. Computational domain and mesh arrangement.

This investigation utilized the Ansys CFX (2021 R1) package to carry out the numerical simulation, and the turbulence k-ε model (realizable with scalable wall functions) and the inlet profile defined by Equations (5)–(7) were applied. Furthermore, a zero-gauge pressure outlet boundary condition was assigned to the domain outlet, and the symmetry boundary condition was applied to the top boundary. As for the ground, the equivalent roughness height k_S = 1.5 and roughness constant C_S = 0.16 were applied with scalable wall function treatment to reflect the realistic aerodynamic resistance of the terrain vegetation cover, as shown in Equation (2).

Due to the relative simplicity of the 2D mountain profile, the Ansys ICEM (2021 R1) meshing tool was utilized to generate the structure mesh, as shown in Figure 8. Furthermore, the mesh arrangement had a first layer height of 3 m and a maximum cell length of 10 m.

3.3. Numerical Simulation Validation

The boundary conditions and turbulence model applied in this study were also utilized in the wind tunnel and numerical simulation study by Pirooz et al. [16]. This study examined the speedup effect at a bell-shaped hill under varying slopes. The reliability of the current CFD simulations was validated by replicating the published study (Pirooz et al. [16]), and the obtained results were compared with the original ones, as shown in Figure 9. The results show that the wind speedup factor from the conducted simulation (blue line) is almost identical to the published result, with a maximum difference of 5.4% occurring below 1.5 m in height. This highlights the accuracy of the numerical simulations presented in the following discussion.

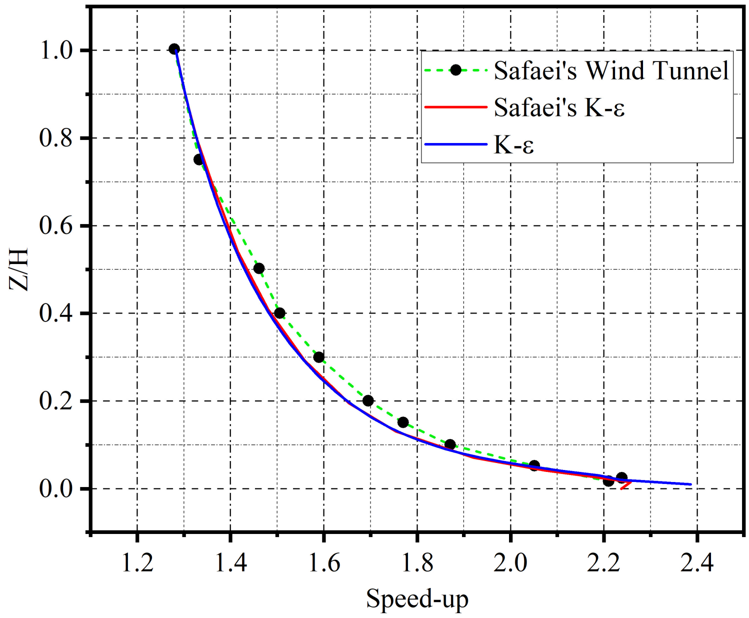

Figure 9. Validation of the numerical simulation accuracy.

A noticeable reduction in the inlet wind velocity and turbulence profile of numerical simulations that employ the k-ε model was reported by Hargreaves et al. [33]. This phenomenon could occur even prior to the presence of an obstacle. To ensure that this did not affect the findings reached in this study, a numerical simulation for the same domain was conducted before introducing the mountain profile, and the homogenous development of the wind field throughout the CFD domain was evaluated. The results demonstrate an evident consistency of the wind velocity, turbulence kinetic energy (TKE), and turbulence dissipation rate throughout the domain, as shown in Figure 10. Furthermore, an insignificant variation in the TKE profile emerged as the flow developed, and the maximum value of divergence was around 3.27% which decreased as the height increased.

3.4. 2D Numerical Simulation Results

3.4.1. Wind Profile at the Side Peak

The wind speed profile at the side peak extending from the mountainside is plotted in Figure 11. The figure shows the influence of the present side peak, with different heights, on the wind speed. The plot illustrates that the incoming wind flow from the inlet experiences a speeding-up effect due to the mountain, without the side peak, reaching 9.5% at a height of 100 m (black line). However, the presence of the extending side peak amplified this effect to 28.5% and 37.3% for the 90 and 135 m high side peaks at 10 m above the top, respectively. This significant increase in wind speed critically enhances the wind influence and loads on structures at such a site. Additionally, the speedup factor extracted from the 3D simulation, which includes the entire realistic topography of Dajue Mountain, is compared with the results from the 2D simulation. The calculation shows a maximum difference of around 10% between the two, which falls to 7% under a height of 200 m. Considering the variations that may occur due to the surrounding topography and the minor differences in results between Ansys Fluent and Ansys CFX, maximum variations of 10% and 7% verify the accuracy of the 3D numerical simulations conducted in Section 2.

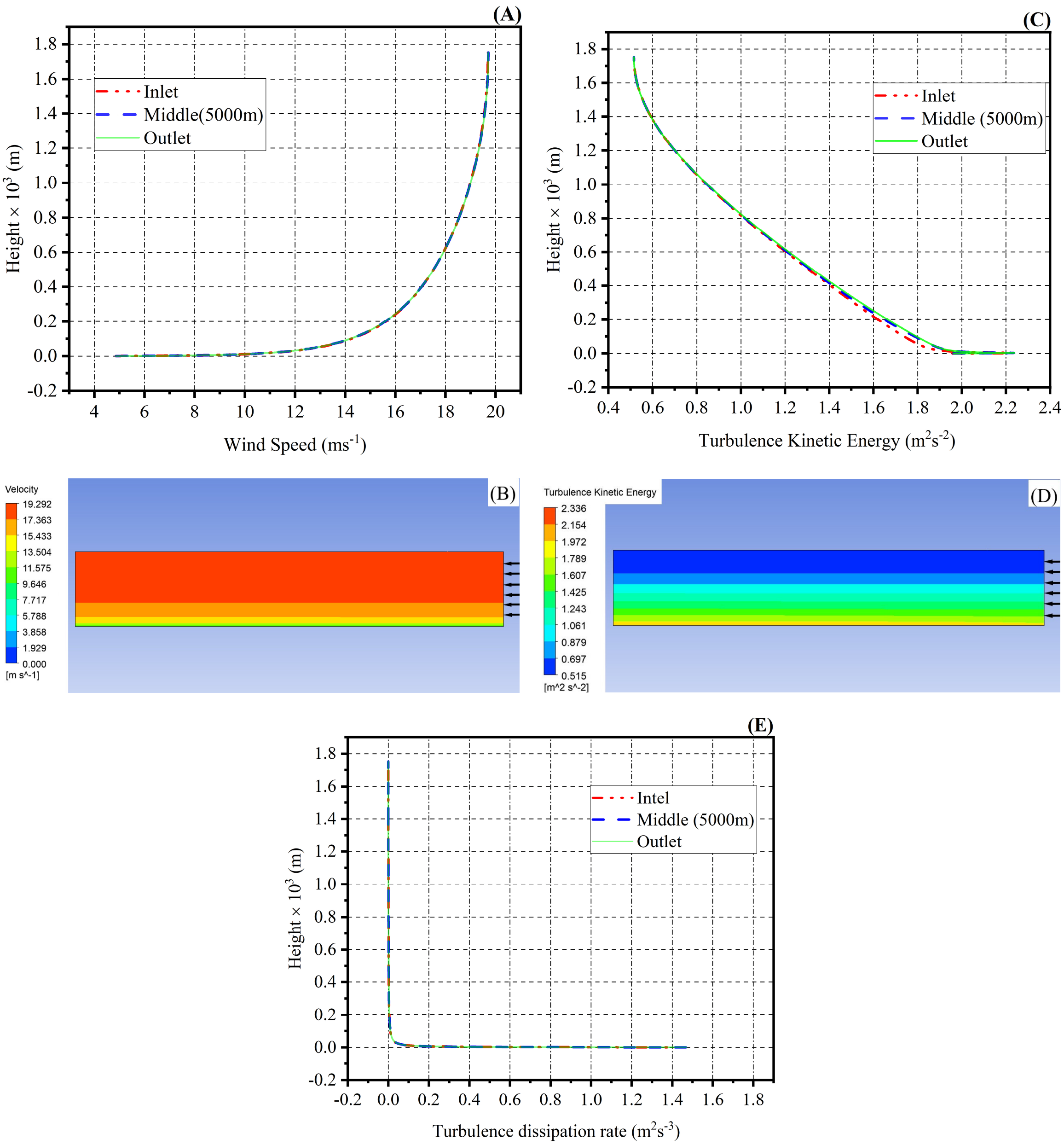

Figure 10. Horizontal homogeneity of the ABL: (**A**) wind speed; (**B**) wind speed development through empty domain; (**C**) TKE; (**D**) TKE development through empty domain; (**E**) turbulence dissipation rate.

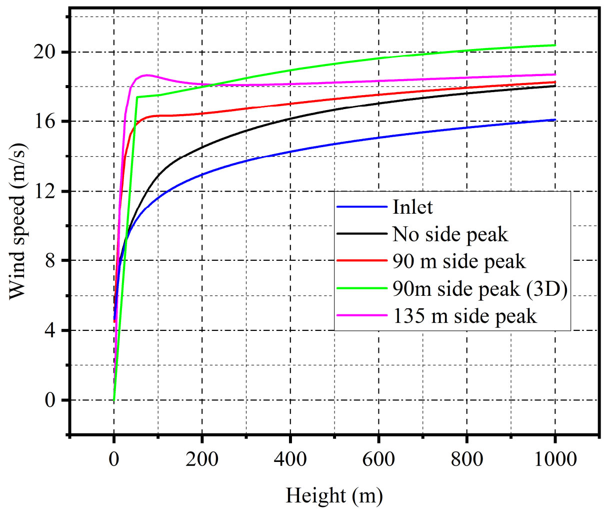

Figure 11. Wind speed profile for different height side peaks.

3.4.2. Speedup Effect at the Mountain Peak

The ability of different wind load standards to predict the speedup effect at the mountain peak is evaluated via comparison with the numerical simulation findings, as shown in Figure 12. The result reveals significant variations between the numerically obtained speedup factors and the recommendations, especially under 50 m high. However, the speedup factor predictions of the ASCE (2022) and AS/NZ (2021) standards over 50 m closely agree with the simulation result.

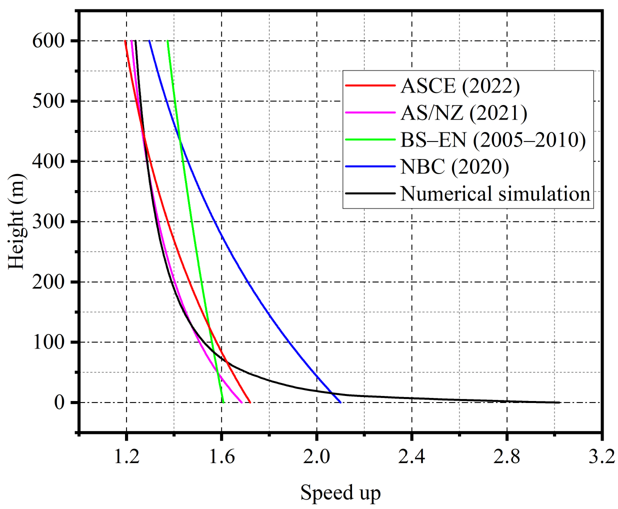

Figure 12. Speedup profile at the mountain peak.

3.4.3. Effect of Different Mountainside Slopes

The mountainside slope directly affects the wind speedup phenomenon, especially near the mountain surface. Figure 13 compares the speedup factor at the position of the side peak after being replaced with a straight line of the same mountain slope under three different slopes; 0.2, 0.31 (original slope), and 0.5. The result shows that under around 25 m, the speedup effect decreases and then surges again; this occurred due to the presence of the short crest before the measurement position, which causes a shading effect.

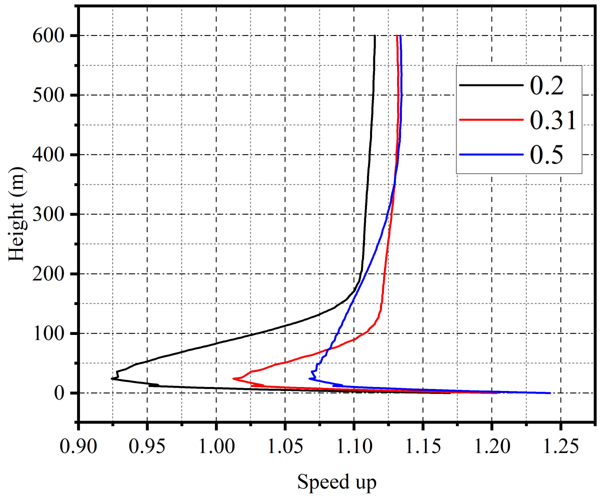

Figure 13. Speedup profile for different mountainside steepness.

Additionally, the difference in the speedup effect of various slopes did not surpass 14% and diminished as the height increased.

3.4.4. Effect of Different Side Peak Heights

Another factor that significantly affects the occurrence of a speedup effect is the presence and height of the side peak. The effects of various side peak heights under different mountainside slopes are plotted in Figure 14. The plots illustrate the significant impact of the side peak on the speedup factor, which led to an increase of approximately 60% near the surface. Additionally, as the height of the side peak increased by 45 m, the speedup factor increased by about 10%. Furthermore, the impact of the side peak on the speedup factor diminishes as the mountainside slope increases. This is attributed to the overall speeding effect caused by the mountain, which, under a certain height, increases with the mountainside slope. This overall speeding effect reduces the significance of the local speedup effect by the side peak.

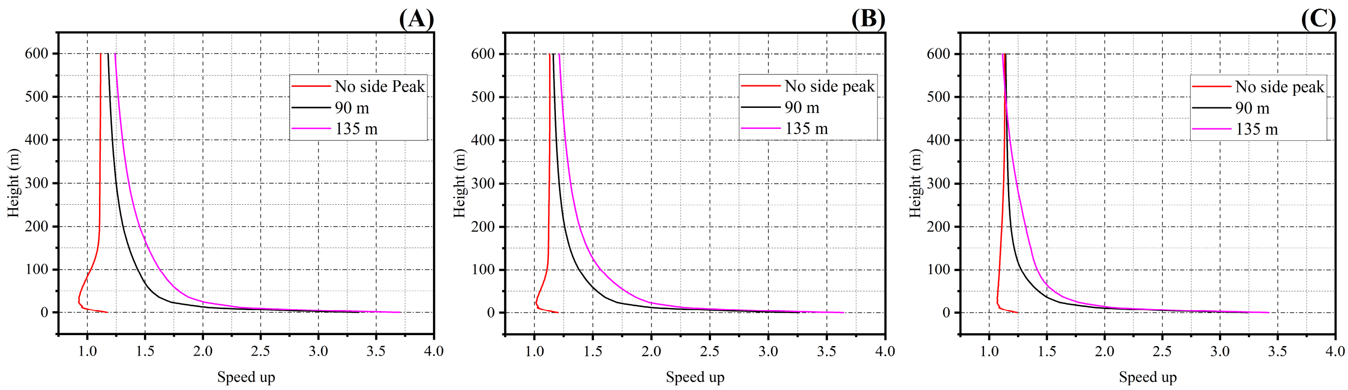

Figure 14. Speedup profile of different side peak heights with various mountainside slopes: (**A**) 0.2; (**B**) 0.31; (**C**) 0.5.

3.4.5. Comparison with Different National Wind Load Standards

The wind speedup factors obtained from the numerical simulation and the recommendations of various wind load specifications are compared in Figure 15. The figure illustrates the speedup effect of the 90 and 135 m high side peaks with different mountainside slopes.

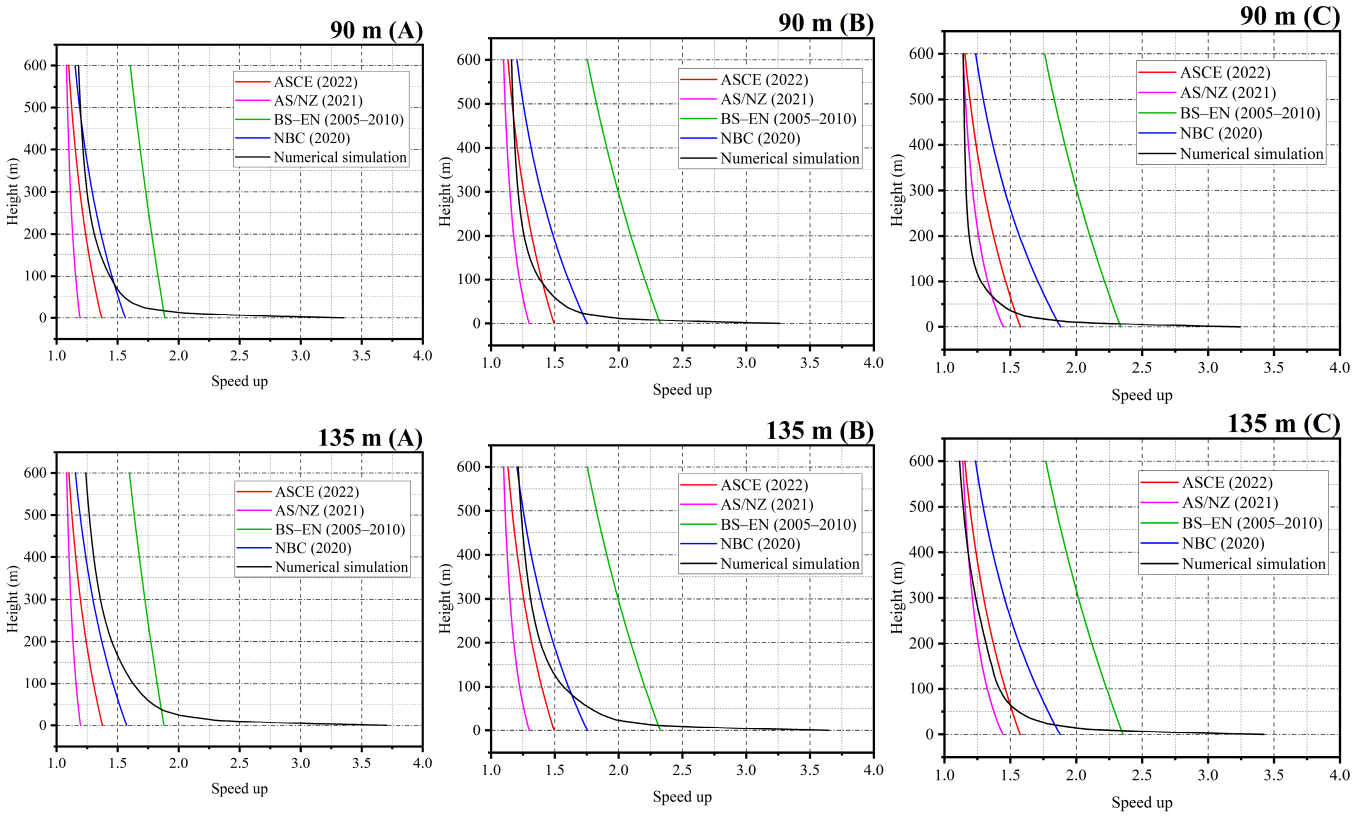

Figure 15. Comparison between the speedup effect of CFD and various national wind load codes under different mountainside slopes: (**A**) 0.2; (**B**) 0.31; (**C**) 0.5.

It is evident that the speedup factor suggested by the standards differs significantly from the simulation results, especially near the peak. Furthermore, apart from BS-EN (2005–2010), these variations diminish with increasing height. Therefore, a thorough evaluation of the wind speedup effect is highly recommended when installing structures at a similar topography. Otherwise, this may result in an unpredictable increase in wind loads, leading to structural damage or, in extreme cases, posing a threat to the safety of occupants or visitors.

4. Conclusions

Numerical simulations have been conducted to investigate the wind flow at a side peak extending out of a mountainside in intricate terrain, where landscape platforms will be installed. The k-e turbulence model was utilized to simulate the wind flow from seven different directions and to evaluate the resulting platforms' wind-induced pressure. This study examined the speedup effect at the towering peak, and the influence of different peak heights and mountainside slopes was explored. The major conclusions of this study are drawn as follows:

- The landscape platforms at the side peak experienced complex patterns of wind pressure due to the influence of surrounding topography, including amplifying and blocking, on the wind and the flow separation around the platforms. This nonuniform wind pressure generates critical torsional and lifting forces that could threaten the structural stability of the platforms.
- The complex terrain substantially amplified the platforms' wind-induced pressure, which in some cases, reached 3.5 times that of when the structure was on flat ground. Therefore, it is crucial to thoroughly evaluate and address this amplifying effect during the design process of structures at such topography, especially lightweight steel structures with complex geometries.

- The investigation of the speedup effect at the towering peak showed that the presence of the peak significantly magnified the speedup effect by approximately 60%, and the variation in the peak height and mountainside steepness has a moderate impact (around 10%) on the resulting speedup factor.
- A comparison of the numerically obtained speedup factor at the side peak and the recommendations of several wind load standards revealed significant variations, especially near the surface. Consequently, further attention should be given to the speedup effect of the actual topography to ensure the accurate assessment of the additional wind load essential for the onsite structure wind resistance design.

Author Contributions: Conceptualization, M.N. and G.F; methodology, M.N.; software, M.N.; validation, L.J. and Z.Y.; formal analysis, M.N.; resources, F.G.; writing—original draft preparation, M.N.; writing—review and editing, M.N. and F.G.; visualization, M.N. and Q.L.; supervision, F.G.; project administration, Q.L. and L.J.; funding acquisition, F.G. and Z.Y. All authors have read and agreed to the published version of the manuscript.

Funding: This research was funded by Zhuzhou CRRCTK under project No: 738011925, focused on the development of the Monorail Elevated Steel Structure Rapid Transit System.

Data Availability Statement: Data will be made available on request.

Conflicts of Interest: The authors affirm that they do not possess any known conflicting financial interests or personal relationships that could have potentially influence the findings presented in this study.

References

1. Hu, W.; Yang, Q.; Chen, H.P.; Yuan, Z.; Li, C.; Shao, S.; Zhang, J. Wind field characteristics over hilly and complex terrain in turbulent boundary layers. *Energy* **2021**, *224*, 120070. [CrossRef]
2. Song, J.; Li, J.W.; Flay, R.G.J.; Pirooz, A.A.S.; Fu, J.Y. Validation and application of pressure-driven RANS approach for wind parameter predictions in mountainous terrain. *J. Wind Eng. Ind. Aerodyn.* **2023**, *240*, 105483. [CrossRef]
3. Blocken, B.; Hout, A.; Dekker, J.; Weiler, O. CFD simulation of wind flow over natural complex terrain: Case study with validation by field measurements for Ria de Ferrol, Galicia, Spain. *J. Wind Eng. Ind. Aerodyn.* **2015**, *147*, 43–57. [CrossRef]
4. Moreira, G.A.; Dos Santos, A.A.; Do Nascimento, C.A.; Valle, R.M. Numerical study of the neutral atmospheric boundary layer over complex terrain. *Boundary-Layer Meteorol.* **2012**, *143*, 393–407. [CrossRef]
5. Han, Y.; Lian, S.; Xu, G.; Cai, C.S.; Hu, P.; Zhang, J. Multiscale simulation of wind field on a long-span bridge site in mountainous area. *J. Wind Eng. Ind. Aerodyn.* **2018**, *177*, 260–274. [CrossRef]
6. Chen, X.; Liu, Z.; Wang, X.; Chen, Z.; Xiao, H.; Zhou, J. Experimental and Numerical Investigation of Wind Characteristics over Mountainous Valley Bridge Site Considering Improved Boundary Transition Sections. *Appl. Sci.* **2020**, *10*, 751. [CrossRef]
7. Liu, Z.; Ishihara, T.; Tanaka, T.; He, X. LES study of turbulent flow fields over a smooth 3-D hill and a smooth 2-D ridge. *J. Wind Eng. Ind. Aerodyn.* **2016**, *153*, 1–12. [CrossRef]
8. Abdi, D.; Bitsuamlak, G.T. Wind flow simulations on idealized and real complex terrain using various turbulence models. *Adv. Eng. Softw.* **2014**, *75*, 30–41. [CrossRef]
9. Yan, S.; Shi, S.; Chen, X.; Wang, X.; Mao, L.; Liu, X. Numerical simulations of flow interactions between steep hill terrain and large scale wind turbine. *Energy* **2018**, *153*, 740–747. [CrossRef]
10. Cunden, T.S.M.; Doorga, J.; Lollchund, M.R.; Rughooputh, S.D.D.V. Multi-level constraints wind farms siting for a complex terrain in a tropical region using MCDM approach coupled with GIS. *Energy* **2020**, *211*, 118533. [CrossRef]
11. Miller, C.; Gibbons, M.; Beatty, K.; Boissonnade, A. Topographic Speed-Up Effects and Observed Roof Damage on Bermuda following Hurricane Fabian (2003). *WAF* **2013**, *28*, 159–174. [CrossRef]
12. Conan, B.; Chaudhari, A.; Aubrun, S.; Beeck, J.V.; Hamalainen, J.; Hellsten, A. Experimental and Numerical Modelling of Flow over Complex Terrain: The Bolund Hill. *Boundary-Layer Meteorol.* **2016**, *158*, 183–208. [CrossRef]
13. Parkinson, D.D.; Pirooz, A.A.S.; Flay, R.G.J. Investigation of Speed-up in Atmospheric Boundary Layer Flow Over Two-dimensional Complex Terrain. In Proceedings of the 21st Australasian Fluid Mechanics Conference, Adelaide, Australia, 10–13 December 2018.
14. Flay, R.G.J.; King, A.B.; Revell, M.; Carpenter, P.; Turner, R.; Cenek, P.; Pirooz, A.A.S. Wind speed measurements and predictions over Belmont Hill, Wellington, New Zealand. *J. Wind Eng. Ind. Aerodyn.* **2019**, *195*, 104018. [CrossRef]
15. Chen, F.; Wang, W.; Gu, Z.; Zhu, Y.; Li, Y.; Shu, Z. Investigation of hilly terrain wind characteristics considering the interference effect. *J. Wind Eng. Ind. Aerodyn.* **2023**, *241*, 105543. [CrossRef]
16. Pirooz, A.A.S.; Flay, R.G.J. Comparison of Speed-Up Over Hills Derived from Wind-Tunnel Experiments, Wind-Loading Standards, and Numerical Modelling. *Boundary-Layer Meteorol.* **2018**, *168*, 213–246. [CrossRef]

17. Zhao, Y.; Li, R.; Feng, L.; Wu, Y.; Niu, J.; Gao, N. Boundary layer wind tunnel tests of outdoor airflow field around urban buildings: A review of methods and status. *Renew. Sust. Energ. Rev.* **2022**, *167*, 112717. [CrossRef]
18. Ricci, A.; Burlando, M.; Freda, A.; Repetto, M.P. Wind tunnel measurements of the urban boundary layer development over a historical district in Italy. *Build. Environ.* **2017**, *111*, 192–206. [CrossRef]
19. Shi, L.; Tao, L.; Zhang, Y.; Li, Y.; Jiang, X.; Yang, Z.; Qi, X.; Qiu, J. CFD simulations of wind-driven rain on typical football stadium configurations in China's hot-summer and cold-winter zone. *Build. Environ.* **2022**, *225*, 109598. [CrossRef]
20. Meng, M.; Tamura, T.; Katsumura, A.; Fugo, Y. LES application to wind pressure prediction for tall building on complex terrain. *J. Wind Eng. Ind. Aerodyn.* **2023**, *242*, 105582. [CrossRef]
21. Han, Y.; Chun, Q.; Xu, X.; Teng, Q.; Dong, Y.; Lin, Y. Wind effects on Chinese traditional timber buildings in complex terrain: The case of Baoguo Temple. *J. Build. Eng.* **2022**, *59*, 105088. [CrossRef]
22. An, L.; Jung, S. Experimental investigation on influence of terrain complexity for wind pressure of low-rise building. *J. Build. Eng.* **2024**, *83*, 108350. [CrossRef]
23. Blocken, B.; Stathopoulos, T.; Carmeliet, J. CFD simulation of the atmospheric boundary layer: Wall function problems. *Atmos. Environ.* **2007**, *41*, 238–252. [CrossRef]
24. *JTG/T 3360-01*; Wind-Resistant Design Specification for Highway Bridges. Ministry of Communications of PRC: Beijing, China, 2018.
25. Deaves, D.M.; Harris, R.I. *A Mathematical Model of the Structure of Strong Winds*; Construction Industry Research and Information Association: London, UK, 1978; Report 76.
26. Richards, P.J.; Norris, S.E. Appropriate boundary conditions for a pressure driven boundary layer. *J. Wind Eng. Ind. Aerodyn.* **2015**, *142*, 43–52. [CrossRef]
27. *AS/NZS1170.2*; Australia/New Zealand Standard, Structural Design Actions, Part 2: Wind Actions, 3d ed. Standards Australia Limited/the Crown in Right of New Zealand: Sydney, New Zealand, 2021; pp. 30–40.
28. *NR24-28-2018*; National Building Code of Canada, volume 1, 15th ed. National Research Council of Canada (NRC): Ottawa, ON, Canada, 2020; 4-32/33.
29. *EN 1991-1-4 (2005) (English)*; Eurocode 1: Actions on Structures–General Actions–Part 1-4: Wind Actions. European Committee for Standardization (CEN): Brussels, Belgium, 2004; pp. 97–102.
30. *BS NA EN 1991-1-4 (2010) (English)*; UK National Annex to Eurocode 1. Actions on Structures. General Actions. Wind Actions. British Standards Institution (BSI): London, UK, 2008; p. 21.
31. *ASCE/SEI 7-22*; Minimum Design Loads and Associated Criteria for Buildings and Other Structures. American Society of Civil Engineers: Reston, Virginia, 2022; pp. 275–277.
32. Wang, Z.; Zou, Y.; Yue, P.; He, X.; Liu, L.; Luo, X. Effect of Topography Truncation on Experimental Simulation of Flow over Complex Terrain. *Appl. Sci.* **2022**, *12*, 2477. [CrossRef]
33. Hargreaves, D.M.; Wright, N.G. On the use of the k–ε model in commercial CFD software to model the neutral atmospheric boundary layer. *J. Wind Eng. Ind. Aerodyn.* **2007**, *95*, 355–369. [CrossRef]